Inorg. Chem. **2004**, *43*, 4415–4426

Controlled Redox Conversion of New X-ray-Characterized Mono- and Dinuclear Heptacoordinated Mn(II) Complexes into Di-μ-oxo-dimanganese Core Complexes

Christelle Hureau,[†] Sébastien Blanchard,[†,‡] Martine Nierlich,[§] Guillaume Blain,[†] Eric Rivière,[†] Jean-Jacques Girerd,[†] Elodie Anxolabéhère-Mallart,*[,†] and Geneviève Blondin*[,†]

Laboratoire de Chimie Inorganique, UMR 8613, LCR-CEA n°33V, Institut de Chimie Moléculaire et des Matériaux d'Orsay, Université Paris-Sud, 91405 Orsay Cedex, and DRECAM/SCM, CEA Saclay, Bâtiment 125, 91191 Gif-sur-Yvette Cedex, France

Received November 18, 2003

Two heptacoordinated Mn(II) complexes are isolated and X-ray characterized using the well-known tpen ligand (tpen = *N*,*N*,*N*′,*N*′-tetrakis(2-pyridylmethyl)-1,2-ethanediamine): [(tpen)Mn(OH$_2$)](ClO$_4$)$_2$ (**1**(ClO$_4$)$_2$) and [(tpen)Mn-(μ-OAc)Mn(tpen)](ClO$_4$)$_3$·2H$_2$O (**2**(ClO$_4$)$_3$·2H$_2$O). Crystallographic data for **1**(ClO$_4$)$_2$ at 110(2) K (respectively at 293-(2) K): monoclinic, space group *C*2/*c*, a = 15.049(3) Å (15.096(3) Å), b = 9.932(2) Å (10.105(2) Å), c = 19.246(4) Å (19.443(4) Å), β = 94.21(3)° (94.50(3)°), Z = 4. Crystallographic data for **2**(ClO$_4$)$_3$·0.5(C$_2$H$_5$)$_2$O at 123(2) K: triclinic, space group $P\bar{1}$, a = 12.707(3) Å, b = 12.824(3) Å, c = 19.052(4) Å, α = 102.71(3)°, β = 97.83(3)°, γ = 98.15(3)°, Z = 2. Investigation of the variation upon temperature of the molar magnetic susceptibility of compound **2**(ClO$_4$)$_3$·2H$_2$O reveals a weak antiferromagnetic exchange interaction between the two high-spin Mn(II) ions (J = –0.65 ± 0.05 cm^{-1}, $H = -J\hat{S}_1\cdot\hat{S}_2$). EPR spectra are recorded on powder samples and on frozen acetonitrile solutions, demonstrating the maintenance upon dissolution of the heptacoordination of Mn in complex **1** while complex **2** partially dissociates. Electrochemical responses of complexes **1** and **2** are investigated in acetonitrile, and bulk electrolyses are performed at oxidative potential in the presence of various amounts of 2,6-lutidine (0–2.65 equiv per Mn ion). The formation from either **1** or **2** of the mixed-valent complex [(tpen)Mn^{III}(μ-O)$_2$Mn^{IV}(tpen)]$^{3+}$ (**3**) is established from mass spectrometry and EPR and IR spectroscopy measurements. When reaction is started from **2**, formation of [(tpen)Mn^{IV}(μ-O)$_2$(μ-OAc)Mn^{IV}]$^{3+}$ (**4**) is evidenced from cyclic voltammetry, EPR, and UV–vis data. The Mn vs tpen ratio in the electrogenerated complexes is accurately controlled by the quantity of additional 2,6-lutidine. The role of tpen as a base is discussed.

Introduction

Manganese is known to be involved in the active sites of several redox metalloenzymes such as superoxide dismutase (SOD),[1] catalase,[2−4] and the oxygen evolving complex (OEC) in photosystem II (PSII).[5−8] The first two systems are well documented. For the SOD, high-resolution X-ray structures are available and the mechanisms of the dismutation of the superoxide radical have been proposed.[1] High-resolution X-ray structures have been published for the *Thermus thermophilus* and *Lactobacillus plantarum* Mn catalases[9,10]

* Authors to whom correspondence should be addressed. E-mail: gblondin@icmo.u-psud.fr (G.B.); eanxolab@icmo.u-psud.fr (E.A.-M.).
† Université Paris-Sud.
‡ Current address: Max-Plank Institut für Bioanorganische Chemie, Stiftstrasse 34-36, D-45470 Muelheim an der Ruhr, Germany.
§ CEA Saclay.

(1) Whittaker, J. W. *Mn and its role in Biological Processes*; Marcel Dekker: New York, 2000; Vol. 37, pp 587−611.
(2) Dismukes, G. C. *Chem. Rev.* **1996**, *96*, 2909−2926.
(3) Law, N. A.; Caudle, M. T.; Pecoraro, V. L. In *Advances in Inorganic Chemistry*; Sykes, G. B., Ed.; Academic Press: San Diego, 1998; Vol. 46, pp 305−440.
(4) Yoder, D. W.; Hwang, J.; Penner-Hahn, J. E. *Manganese and its role in Biological Processes*; Marcel Dekker: New York, 2000; Vol. 37, pp 527−557.
(5) Larson, E. J.; Pecoraro, V. L. In *Manganese Redox Enzymes*; Pecoraro, V. L., Ed.; VCH Publishers: New York, 1992; pp 1−28.
(6) Yachandra, V. K.; Sauer, K.; Klein, M. P. *Chem. Rev.* **1996**, *96*, 2927−2950.
(7) Barber, J.; Anderson, J. M. *Philos. Trans.: Biol. Sci.* **2002**, *357*.
(8) Ferreira, K. N.; Iverson, T. M.; Maghlaoui, K.; Barber, J.; Iwata, S. *Science* **2004**, *303*, 1831−1838.
(9) Antonyuk, S. V.; Melik-Adamyan, V. R.; Popov, A. N.; Lamzin, V. S.; Hempstead, P. D.; Harrison, P. M.; Artymiuk, P. J.; Barynin, V. V. *Cryst. Rep.* **2000**, *45*, 105−116.

10.1021/ic035332u CCC: $27.50
Published on Web 06/09/2004

along with possible mechanisms for the dismutation of hydrogen peroxide. In particular, it has been demonstrated that manganese swings between the +II and +III oxidation states. On the reverse, the OEC is still a mysterious machinery. Resolution of the recently published X-ray diffraction studies[8,11,12] is still too low to allow the determination of the structure of the tetranuclear Mn−oxo cluster[13,14] that is responsible for the oxidation of water into dioxygen. This reaction requires four oxidizing equivalents, which are stored one by one under light by the OEC.[15] Kok et al. have proposed that the OEC goes through five oxidation states, denoted S_0 to S_4, dioxygen being released in the S_4 to S_0 transition.[16] On the basis of X-ray absorption techniques and EPR spectroscopy performed on the S_{0-3} states,[6,15,17−20] it is proposed that the manganese ions are present under the +II, +III, and/or +IV oxidation states. Furthermore, mechanistic proposals for the oxidation of water do not exclude a transitory Mn(V) center or a Mn(IV)−oxyl radical in the unstable S_4 state.[21−24]

The ability to store four oxidizing equivalents is required for any artificial system designed for the catalytic oxidation of water into dioxygen. Consequently, investigation of the evolution of low-valent Mn complexes under oxidative conditions is of great interest with respect to artificial photosynthesis.[25−28] For instance, the interconversion among $[Mn^{III}_2(\mu\text{-O})(\mu\text{-OAc})_2]^{2+}$, $[Mn^{III}Mn^{IV}(\mu\text{-O})_2(\mu\text{-OAc})]^{2+}$, and $[Mn^{IV}_2(\mu\text{-O})_2(\mu\text{-OAc})]^{3+}$ core complexes has been studied.[29,30] Dismutation processes in acidic medium have been evidenced together with the effect of additional acetate ions. Only a few investigations have been performed involving Mn(II) complexes.[31−35] In these published works, the starting complexes were mononuclear and the ligands bidentate 2,2′-bipyridine (bpy), tridentate 2,2′:6,2″-terpyridine (terpy), or *N*,*N*-bis(2-pyridylmethyl)ethylamine (bpea). The dinuclear $Mn^{II}Mn^{II}$ complex was also investigated with the bpea ligand.[30] It was shown that condensation processes under oxidative potentials require the presence of an exogenous ligand such as acetate or a buffered medium using the ligand itself to stabilize the generated Mn−oxo species. It is worth noting that the involved ligands exhibit a univocal coordination mode, i.e., bi- or tridentate on a single metal ion.

We report here the evolution under bulk electrolysis of two Mn(II) complexes synthesized with *N*,*N*,*N*′,*N*′-tetrakis-(2-pyridylmethyl)-1,2-ethanediamine (tpen). Three high-valent manganese complexes have been previously X-ray characterized, namely, the mixed-valence $Mn^{III}Mn^{IV}$ complex $[(tpen)Mn_2(\mu\text{-O})_2(\mu\text{-OAc})]^{2+}$ [36] and the two Mn(IV)-based cations $[(tpen)Mn_2(\mu\text{-O})_2(\mu\text{-OAc})]^{3+}$ and $[\{(tpen)(OH)Mn_3(\mu\text{-O})_4\}_2(\mu\text{-tpen})]^{6+}$.[37] The room-temperature X-ray structure of $[(tpen)Mn(OH_2)]^{2+}$ (**1**) has been reinvestigated,[38] and new data recorded at 110 K are presented, both showing a heptacoordinated Mn(II) ion. X-ray diffraction studies of $[(tpen)Mn(\mu\text{-OAc})Mn(tpen)]^{3+}$ (**2**) presented here reveal in addition to heptacoordinated Mn(II) ions an unusual *anti*−*anti* bridging mode for the acetate anion. The versatility of the tpen ligand indeed allows access to new complexes such as the mixed-valence complex $[(tpen)Mn^{III}(\mu\text{-O})_2Mn^{IV}(tpen)]^{3+}$ (**3**). Furthermore, we show here that tpen also acts as a base and finely tunes the chemical nature of the dimanganese core units formed upon oxidation. This is related to the previously reported synthesis of $[(tpen)Mn_2(\mu\text{-O})_2(\mu\text{-OAc})]^{2+}$.

Experimental Section

Materials. Reagents and solvents were purchased commercially and used as received. Tpen was synthesized according to a previously reported procedure.[39]

Caution: Perchlorate salts of metal complexes with organic ligands are potentially explosive. Only small quantities of these compounds should be prepared and handled behind suitable protective shields.

Syntheses. $[(tpen)Mn(OH_2)](ClO_4)_2$ ($\mathbf{1}(ClO_4)_2$). To a 5 mL methanolic solution of tpen (200 mg, 0.47 mmol) was added a 0.5 mL aqueous solution of $Mn(ClO_4)_2\cdot 6H_2O$ (171 mg, 0.47 mmol). Rapidly, the formation of a pale yellow precipitate was observed. It was filtered, washed with 1 mL of water, and dried with diethyl

(10) Barynin, V. V.; Whittaker, M. M.; Antonyuk, S. V.; Lamzin, V. S.; Harrison, P. M.; Artymiuk, P. J.; Whittaker, J. W. *Structure* **2001**, *9*, 725−738.
(11) Zouni, A.; Witt, H.-T.; Kern, J.; Fromme, P.; Krauss, N.; Saenger, W.; Orth, P. *Nature* **2001**, *409*, 739−743.
(12) Kamiya, N.; Shen, J.-R. *Proc. Natl. Acad. Sci. U.S.A.* **2002**, *100*, 98−103.
(13) Rutherford, A. W.; Faller, P. *Trends Biochem. Sci.* **2001**, *26*, 341−344.
(14) Rutherford, A. W.; Boussac, A. *Science* **2004**, *303*, 1782−1784.
(15) Robblee, J. H.; Cinco, R. M.; Yachandra, V. K. *Biochim. Biophys. Acta* **2001**, *1503*, 7−23.
(16) Kok, B.; Forbush, B.; McGloin, M. *Photochem. Photobiol.* **1970**, *11*, 457−475.
(17) Carrell, T. G.; Tyryshkin, A. M.; Dismukes, G. C. *J. Biol. Inorg. Chem.* **2002**, *7*, 2−22.
(18) Dau, H.; Iuzzolino, L.; Dittmer, J. *Biochim. Biophys. Acta* **2001**, *1503*, 24−39.
(19) Geijer, P.; Peterson, S.; Åhrling, K. A.; Deák, Z.; Styring, S. *Biochim. Biophys. Acta* **2001**, *1503*, 83−95.
(20) Peloquin, J. M.; Britt, R. D. *Biochim. Biophys. Acta* **2001**, *1503*, 96−111.
(21) Limburg, J.; Szalai, v.; Brudwig, G. W. *J. Chem. Soc., Dalton Trans.* **1999**, *1999*, 1353−1361.
(22) Vrettos, J. S.; Limburg, J.; Brudvig, G. W. *Biochim. Biophys. Acta* **2001**, *1503*, 229−245.
(23) Siegbahn, P. E. M. *Curr. Opin. Chem. Biol.* **2002**, *6*, 227−235.
(24) Pecoraro, V. L.; Baldwin, M. J.; Caudle, M. T.; Hsieh, W.-Y.; Law, N. A. *Pure Appl. Chem.* **1998**, *70*, 925−929.
(25) Sun, L.; Hammarström, L.; Åkermark, B.; Styring, S. *Chem. Soc. Rev.* **2001**, *30*, 36−49.
(26) Burdinski, D.; Bothe, E.; Wieghardt, K. *Inorg. Chem.* **2000**, *39*, 105−116.
(27) Burdinski, D.; Wieghardt, K.; Steenken, S. *J. Am. Chem. Soc.* **1999**, *121*, 10781−10787.
(28) Johansson, A.; Abrahamsson, M.; Magnuson, A.; Huang, P.; Martensson, J.; Styring, S.; Hammarström, L.; Sun, L.; Åkermark, B. *Inorg. Chem.* **2003**, *42*, 7502−7511.
(29) Lal, T. K.; Mukherjee, R. *Inorg. Chem.* **1998**, *37*, 2373−2382.
(30) Romero, I.; Dubois, L.; Collomb, M.-N.; Deronzier, A.; Latour, J.-M.; Pécaut, J. *Inorg. Chem.* **2002**, *41*, 1795−1806.
(31) Morrison, M. M.; Sawyer, D. T. *Inorg. Chem.* **1978**, *17*, 333−337.
(32) Collomb Dunand-Sauthier, M.-N.; Deronzier, A.; Romero, I. *J. Electroanal. Chem.* **1997**, *436*, 219−225.
(33) Collomb Dunand-Sauthier, M.-N.; Deronzier, A.; Pradon, X. *J. Am. Chem. Soc.* **1997**, *119*, 3173−3174.
(34) Collomb Dunand-Sauthier, M.-N.; Deronzier, A.; Piron, A.; Pradon, X.; Ménage, S. *J. Am. Chem. Soc.* **1998**, *120*, 5373−5380.
(35) Baffert, C.; Collomb, M.-N.; Deronzier, A.; Pécaut, J.; Limburg, J.; Crabtree, R. H.; Brudvig, G. W. *Inorg. Chem.* **2002**, *41*, 1404−1411.
(36) Pal, S.; Gohdes, J. W.; Wilisch, W. C. A.; Armstrong, W. H. *Inorg. Chem.* **1992**, *31*, 713−716.
(37) Pal, S.; Armstrong, W. H. *Inorg. Chem.* **1992**, *31*, 5417−5423.
(38) Lee, J.-D.; Lee, M.-H. *J. Ind. Eng. Chem.* **2001**, *7*, 137−142.
(39) Toftlund, H.; Yde-Andersen, S. *Acta Chem. Scand.* **1981**, *A35*, 575.

Table 1. Crystallographic Data for **1**$(ClO_4)_2$ and for **2**$(ClO_4)_3 \cdot 0.5(C_2H_5)_2O$

empirical formula	$MnC_{26}H_{30}Cl_2N_6O_9$	$MnC_{26}H_{30}Cl_2N_6O_9$[a]	$Mn_2C_{56}H_{64}N_{12}O_{14.5}Cl_3$
fw	696.40	696.40	1353.42
temp (K)	110(2)	293(2)	123(2)
wavelength (Å)	0.71073	0.71073	0.71073
cryst syst	monoclinic	monoclinic	triclinic
space group	*C*2/*c*	*C*2/*c*	$P\bar{1}$
a, Å	15.049(3)	15.096(3)	12.707(3)
b, Å	9.932(2)	10.105(2)	12.824(3)
c, Å	19.246(4)	19.443(4)	19.052(4)
α, deg	90.	90.	102.71(3)
β, deg	94.21(3)	94.50(3)	97.83(3)
γ, deg	90.	90.	98.15(3)
V, Å^3	2869(1)	2957(1)	2952(1)
Z	4	4	2
ρ_{calcd}, g.cm^{-3}	1.612	1.564	1.522
μ, mm^{-1}	0.712	0.690	0.641
R1[b]	0.0347	0.0434	0.0491
wR2[c]	0.0805	0.0979	0.1612

[a] In ref 29, the structural characteristics were the following: crystallographic system monoclinic, space group *Cc*, $a = 15.087(3)$ Å, $b = 10.108(2)$ Å, $c = 19.444(3)$ Å, $\beta = 94.58(1)°$. [b] $R1 = \sum||F_o| - |F_c||/\sum|F_o|$. [c] $wR2 = \{\sum[w(F_o^2 - F_c^2)^2]/\sum[w(F_o^2)^2]\}^{1/2}$.

ether. A 200 mg sample of $[(tpen)Mn(OH_2)](ClO_4)_2$ was collected (yield 61%). Crystals suitable for X-ray diffraction studies were obtained by slow evaporation of a saturated methanolic solution of **1**$(ClO_4)_2$. Anal. Calcd for $C_{26}H_{30}N_6O_9Cl_2Mn$: C, 44.8; H, 4.3; N, 12.1; Cl, 10.2; Mn, 7.9. Found: C, 45.1; H, 4.4; N, 12.2; Cl, 10.0; Mn, 7.7.

[(tpen)Mn(*μ*-OAc)Mn(tpen)](ClO$_4$)$_3$·2H$_2$O (2(ClO$_4$)$_3$·2H$_2$O). Tpen (200 mg, 0.47 mmol, 1 equiv) was allowed to react with $Mn(OAc)_2 \cdot 4H_2O$ (140 mg, 0.57 mmol, 1.2 equiv) in 4 mL of methanol in the presence of a slight excess of sodium acetate (77 mg, 0.94 mmol, 2 equiv). After the reaction mixture was stirred for 30 min, $NaClO_4$ was added (173 mg, 1.41 mmol, 3 equiv). After 5 days, the pale yellow precipitate was filtered, washed with methanol, and dried with diethyl ether. A 257 mg sample of $[(tpen)Mn(\mu\text{-}OAc)Mn(tpen)](ClO_4)_3 \cdot 2H_2O$ was collected (yield 40%). Crystals suitable for X-ray diffraction studies were obtained by slow diffusion of diethyl ether into a saturated acetonitrile solution of **2**$(ClO_4)_3 \cdot 2H_2O$. Anal. Calcd for $C_{54}H_{63}N_{12}O_{16}Cl_3Mn_2$: C, 48.0; H, 4.7; N, 12.4; Cl, 7.9; Mn, 8.1. Found: C, 48.0; H, 4.6; N, 12.5; Cl, 7.9; Mn, 8.2.

[(tpen)Mn$_2$(*μ*-O)$_2$(*μ*-OAc)](ClO$_4$)$_2$·3H$_2$O. This compound was prepared for the purpose of infrared spectroscopy result comparisons. It was synthesized according to the previously published procedure.[36]

Infrared Spectroscopy. Spectra were recorded on KBr pellets in the range from 4000 to 200 cm^{-1} with a Perkin-Elmer Spectrum 1000 spectrophotometer.

Electrospray Ionization Mass Spectrometry. Mass spectra were recorded using the centroid detection mode with a Finnigan Mat Mat95S in a BE configuration at low resolution on millimolar acetonitrile solutions.

Elemental Analysis. Analyses were performed by the Service de Microanalyse of the CNRS (Gif-sur-Yvette, France) for carbon, nitrogen, and hydrogen and by the Service Central d'Analyse of CNRS (Vernaison, France) for manganese and chloride.

Crystallographic Data Collection and Refinement of the Structures of 1(ClO$_4$)$_2$ and 2(ClO$_4$)$_3$·0.5(C$_2$H$_5$)$_2$O. Crystals of approximate dimensions of 0.15 × 0.10 × 0.05 mm for **1**$(ClO_4)_2$ and 0.20 × 0.15 × 0.10 mm for **2**$(ClO_4)_3 \cdot 0.5(C_2H_5)_2O$ were selected. Diffraction collections were carried out on a Nonius diffractometer equipped with a CCD detector. The lattice parameters were determined from 10 images recorded with 2° *ϕ*-scans and later refined on all data. The data were recorded at 123 K for **2**$(ClO_4)_3 \cdot 0.5(C_2H_5)_2O$ and 110 and 293 K for **1**$(ClO_4)_2$. A 180° *ϕ*-range was scanned, with 2° steps, with the crystal-to-detector distance fixed at 30 mm. The data were corrected for Lorentz polarization effects. The structures were solved by the heavy atom method and refined by the full-matrix least-squares method on F^2 with anisotropic thermal parameters for all non-H atoms and solvent atoms. H atoms were introduced at calculated positions and constrained to reside on their parent C atom. All calculations were performed on an O2 Silicon Graphics Station with the SHELXTL package.[40,41] The crystallographic data are given in Table 1.

Magnetic Susceptibility Measurements. Magnetic susceptibility data were recorded on an MPMS5 magnetometer (Quantum Design Inc.). The calibration was made at 298 K using a palladium reference sample furnished by Quantum Design Inc. The data were collected over a temperature range of 2−300 K. Above 100 K, a 1 T magnetic field was applied, while below 100 K, the amplitude was 0.05 T. The sample holder was independently measured and its contribution subtracted. The data were further corrected for diamagnetism using Pascal's constants.

EPR Spectroscopy. X-band EPR spectra were recorded on a Bruker ELEXSYS 500 (X- and Q-band) spectrometer using the conventional perpendicular detection mode. For low-temperature studies, an Oxford Instrument continuous flow liquid helium cryostat and a temperature control system were used. All the simulations were performed using the XSophe software (4.0 version) developed by the Department of Mathematics at the University of Queensland, Brisbane, Australia.

Cyclic Voltammetry and Bulk Electrolysis. Cyclic voltammetry and coulometry measurements were recorded on an EGG PAR potentiostat (M273 model). The counter electrode was a Au wire and the working electrode a glassy carbon disk carefully polished before each voltammogram with a 1 μm diamond paste, sonicated in an ethanol bath, and then washed carefully with ethanol. It is worth noting that, in the absence of such a treatment of the working electrode surface, the successive cyclic voltammograms were not reproducible. The reference electrode was a 0.01 M $Ag/AgClO_4$ electrode (0.29 V vs SCE and 0.53 V vs NHE), isolated in a fritted bridge. The solvent used was distilled acetonitrile, and tetrabutylammonium perchlorate was added to obtain a 0.1 M supporting electrolyte. This electrolyte solution was further dried over a neutral alumina column.

(40) Sheldrick, G. M. *SHELXTL-97, Program for the refinement of Crystal Structure*; University of Göttingen: Göttingen, Germany, 1997.
(41) Sheldrick, G. M., University of Göttingen, Germany, 1999, distributed by Bruker AXS, Madison, WI.

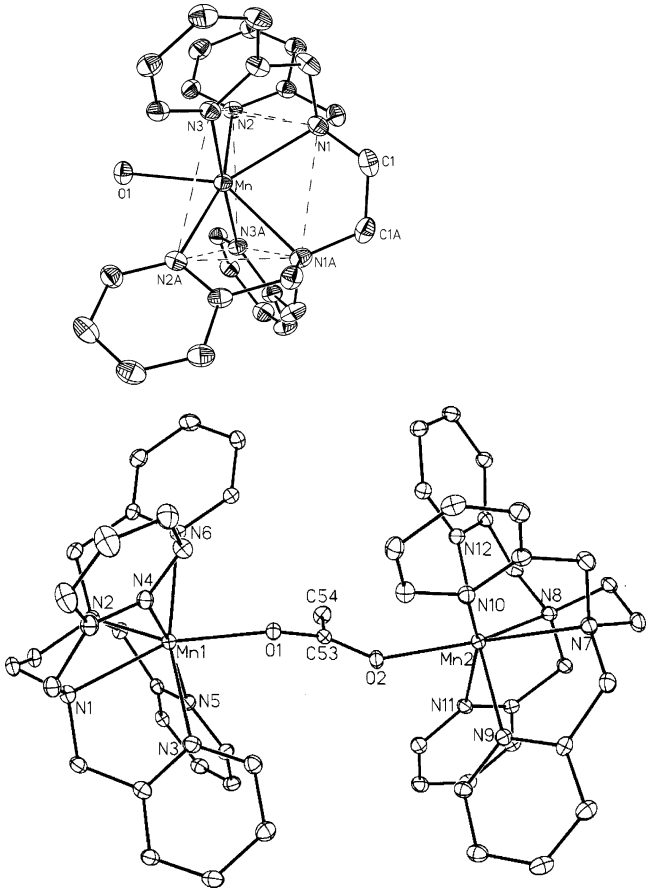

Figure 1. ORTEP view of the cation $[(tpen)Mn(OH_2)]^{2+}$ in $\mathbf{1}(ClO_4)_2$ (top) and of the cation $[(tpen)Mn(\mu\text{-}O_2CCH_3)Mn(tpen)]^{3+}$ in $\mathbf{2}(ClO_4)_3 \cdot 0.5(C_2H_5)_2O$ (bottom). Dashed lines in the top structure define the edges of the trigonal prism.

UV−Vis Spectroscopy. UV−vis spectra were recorded on a Varian Cary 300 Bio or a Varian Cary 5E spectrophotometer at 20 °C with either 0.1 or 1 cm quartz cuvettes.

Results

The mononuclear complex $[(tpen)Mn(OH_2)]^{2+}$ (**1**) and the dinuclear complex $[(tpen)Mn(\mu\text{-}OAc)Mn(tpen)]^{3+}$ (**2**) can be isolated using the well-known tpen ligand. The coordinating ability of the anion in the starting Mn(II) salt controls the nuclearity of the final species.

X-ray Structures. The X-ray data of $\mathbf{1}(ClO_4)_2$ were collected at two different temperatures due to the differences in the EPR signatures (see below). The two structures are the same, and only the one determined at low temperature will be commented on, except where otherwise stated. Figure 1 reproduces the ORTEP view of cations **1** and **2**. The common feature of both complexes is the heptacoordination of the Mn(II) ions. Selected bond lengths and angles are listed in Tables 2 and 3. The Mn−water bond coincides with a C_2 rotation axis in **1**. The molecular geometry around the metal ion is somewhat distorted but is best described as a capped trigonal prism in which the oxygen atom caps the rectangular face defined by four nitrogen atoms, N2N3N2′N3′ in **1** (see dashes at the top of Figure 1) and N3N4N5N6 and N9N10N11N12 in **2**. As can be seen from Table 2, the coordination spheres of the Mn(II) ions are rather irregular,

Table 2. Selected Bond Lengths (Å) and Angles (deg) in **1**

	293 K	110 K	in ref 29[a]
Mn1−O1	2.269(3)	2.259(2)	2.260(4)
Mn1−N1	2.396(3)	2.402(2)	2.414(9), 2.376(11)
Mn1−N2	2.471(3)	2.463(2)	2.423(9), 2.512(9)
Mn1−N3	2.296(3)	2.292(2)	2.307(9), 2.266(10)
O1−Mn1−N1	142.64(7)	142.82(5)	145.5(5), 139.5(5)
O1−Mn1−N2	81.07(7)	80.87(5)	81.7(4), 80.2(4)
O1−Mn1−N3	90.94(7)	90.84(5)	92.0(5), 89.8(4)

[a] No C_2 rotation axis was observed.

Table 3. Selected Bond Lengths (Å) and Angles (deg) in **2**

Mn1−O1	2.149(3)	Mn2−O2	2.129(3)
Mn1−N1	2.409(3)	Mn2−N8	2.388(3)
Mn1−N2	2.404(3)	Mn2−N7	2.433(3)
Mn1−N3	2.394(3)	Mn2−N10	2.389(3)
Mn1−N6	2.398(3)	Mn2−N11	2.466(3)
Mn1−N4	2.287(3)	Mn2−N9	2.252(3)
Mn1−N5	2.337(3)	Mn2−N12	2.344(3)
O1−Mn1−N1	146.45(10)	O2−Mn2−N8	137.49(11)
O1−Mn1−N2	138.72(11)	O2−Mn2−N7	148.55(11)
O1−Mn1−N3	80.61(10)	O2−Mn2−N10	83.05(11)
O1−Mn1−N6	82.05(10)	O2−Mn2−N11	82.08(11)
O1−Mn1−N4	92.49(11)	O2−Mn2−N9	90.91(11)
O1−Mn1−N5	89.71(11)	O2−Mn2−N12	90.30(11)

probably owing to the geometric constraints of the ligand. There are two short $Mn-N_{pyridine}$ bond distances (2.292(2) Å for N3 in **1**, 2.287(3), 2.337(3), 2.252(3), and 2.344(3) Å for N4, N5, N9, and N12 in **2**, respectively) and two long ones (2.463(2) Å for N2 in **1**, 2.394(3), 2.398(3), 2.389(3), and 2.466 Å for N3, N6, N10, and N11 in **2**, respectively). The distortion around the Mn sites in **2** is close to the one observed in **1**. Such a distortion has been previously observed in the first published structure of $\mathbf{1}(ClO_4)_2$.[38] However, the average values for the $Mn-N_{amine}$ and long and short $Mn-N_{pyridine}$ distances can be readily compared among the three structures. The longest $Mn-N_{pyridine}$ bond lengths reported here are significantly greater than the commonly measured ones (2.212−2.424 Å).[42] On the reverse, the $Mn-N_{amine}$ bond lengths are significantly shorter here than the ones published in the literature. The $Mn-O_{acetate}$ and $Mn-O_{water}$ bond distances are similar to the values usually observed in Mn(II) complexes.

The $O-Mn-N_{pyridine}$ angles are close to the expected value of 90° when the pyridine nitrogen atom involved is the most distant from the metallic site. Smaller angle values are indeed found when the $Mn-N_{pyridine}$ distances are shorter. The $O-Mn-N_{amine}$ angles are all in the same range, from 137.49(11)° to 148.55(11)°.

Increasing the temperature from 110 to 293 K induced changes in the Mn−Mn intermolecular distances in $\mathbf{1}(ClO_4)_2$. While at 110 K each manganese ion has four Mn neighbors lying at 9.016 Å, two at 9.679 Å, and two at 9.932 Å, these values increase up to 9.083, 9.784, and 10.105 Å at room temperature, respectively.

If such a distorted capped trigonal prism is usually observed for heptacoordinated Mn(II) ions, this is the first time to our knowledge that it is detected in a dinuclear

(42) Horner, O.; Girerd, J.-J.; Philouze, C.; Tchertanov, L. *Inorg. Chim. Acta* **1999**, *290*, 139−144 and references therein.

system. Furthermore, complex **2** is the third dinuclear complex where the two Mn sites are bridged by a single acetate which presents in addition the atypical *anti*−*anti* coordination mode. In the first two X-ray-characterized [Mn^{II}-(μ-OAc)Mn^{II}]$^{3+}$ core complexes,[43,44] the acetate anion presents a *syn*−*anti* bridging mode, leading to shorter Mn···Mn separations (5.67 and 4.82 Å) than the one reported here (6.341(3) Å).[45] Indeed, comparable Mn···Mn separations of 6.036,[46] 6.335,[47] and 6.555[48] Å are observed in 3D-structure systems where two Mn(II) ions are linked by a carboxylate group in the *anti*−*anti* conformation. When compared to the Mn···Mn separations (6.48−6.52 Å) observed in linear polymeric Mn(III) chains where the *anti*−*anti* bridging mode of the acetate ion is found,[49−51] the 6.341(3) Å Mn···Mn distance determined here is slightly shorter. This may be attributed to the longer Mn−$O_{acetate}$ distance observed in the Mn(III) chains due to the Jahn−Teller effect. The *anti*−*anti* bridging mode of the acetate ion can here be attributed to the steric constriction of the tpen ligand. There is no opening of the O1−C53−O2 angle of the acetate (122.3(3)°). The two planes defined by Mn1−N1−N2−O1 (mean deviation 0.037 Å) and Mn2−N7−N8−O2 (mean deviation 0.020 Å) are slightly twisted (dihedral angle 24(2)°); both form an angle of ±30(3)° with the plane of the acetate bridge.

Magnetic Susceptibility Measurements. The molar magnetic susceptibility was only measured for the dinuclear complex **2**. Crystals of **2**$(ClO_4)_3$·0.5$(C_2H_5)_2O$ were finely crushed to a powder, and the collected data are reproduced in Figure S1 of the Supporting Information as a $\chi_M T$ vs T curve, where χ_M is the molar magnetic susceptibility and T the temperature. The $\chi_M T$ product is rather constant between 300 and 100 K since it varies between 8.41 and 8.30 cm^3 mol^{-1} K. This corresponds well to the 8.75 cm^3 mol^{-1} K expected value for two uncoupled high-spin Mn(II) ions ($S_{Mn(II)} = 5/2$). Below 100 K, $\chi_M T$ decreases more rapidly to reach 2.03 cm^3 mol^{-1} K at 2 K, indicating a weak antiferromagnetic exchange interaction between the two paramagnetic centers. These data can be satisfyingly reproduced by using the van Vleck formula and the exchange Hamiltonian $H = -J\hat{S}_1 \cdot \hat{S}_2$. The best fit was obtained with $g = 1.97$ and $J = -0.65 \pm 0.05$ cm^{-1} (see Figure S1). No zero-field splitting effect on the Mn(II) ions has been considered nor have intermolecular interactions that can contribute to the decrease of the $\chi_M T$ product when the temperature is decreased. A weak antiferromagnetic exchange interaction seems to be a common feature of mono-μ-acetato-bridged dimanganese(II) systems: $J = -0.39$ cm^{-1} and $J = -0.74$ cm^{-1} were determined in [(bpy)$_2$(OH_2)Mn(μ-O_2CCH_2N-$(CH_3)_3$)Mn(OH_2)(bpy)$_2$]$^{3+}$ [44] and in [LMn_2(μ-OAc)]$^{3+}$,[43] respectively. However, on the basis of these data, the influence of the bridging mode of the acetate anion (*anti*−*anti* vs *syn*−*anti*) can hardly be rationalized.

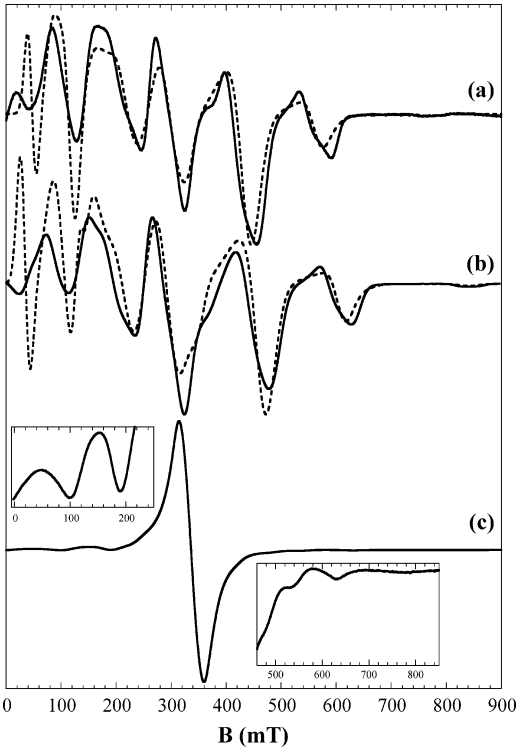

Figure 2. Experimental (solid line) and calculated (dashed line) powder X-band spectra (a, b) of **1**$(ClO_4)_2$ and (c) of **2**$(ClO_4)_3$·$2H_2O$. Recording conditions: microwave power 0.2 mW; modulation amplitude 0.5 mT; modulation frequency 100 kHz; T = 295 K (a), 25 K (b), and 8 K (c); microwave frequency 9.383 GHz (a), 9.386 GHz (b), and 9.388 GHz (c). Insets: zoom on the 0−250 and 460−850 mT regions of spectrum c. See Table 4 for calculated spectra.

EPR Spectroscopy. X-band spectra were recorded on a powder sample of compound **1**$(ClO_4)_2$ between 4 and 300 K. The 25 K and room-temperature spectra are shown in Figure 2 (solid line, parts a and b). The profile is the same as the one reported previously,[38] but the positions of the lines are temperature dependent above 100 K, while they are unchanged when the temperature is decreased below 100 K. When the temperature is decreased from 295 to 100 K, the lines above and below 330 mT are displaced toward higher and lower magnetic fields, respectively. These EPR signals can be well interpreted as originating from an $S = 5/2$ system that presents a zero-field splitting effect competitive with the Zeeman interaction. The spin Hamiltonian used to reproduce the experimental signals is given in eq 1.

$$\hat{H} = g\mu_B \hat{B} \cdot \hat{S} + D\left[\hat{S}_z^2 - \frac{1}{3}\hat{S}^2\right] + E[\hat{S}_x^2 - \hat{S}_y^2] \qquad (1)$$

The first term stands for the electronic Zeeman interaction, while the second and third terms reproduce the zero-field splitting effect. Since the Mn(II) ion presents a d^5 electronic configuration, the Zeeman interaction is assumed to be

(43) Adams, H.; Bailey, N. A.; Debaeker, N.; Fenton, D. E.; Kanda, W.; Latour, J.-M.; Okawa, H.; Sakiyama, H. *Angew. Chem., Int. Ed. Engl.* **1995**, *34*, 2535−2537.
(44) Chen, X.-M.; Tong, Y.-X.; Xu, Z.-T.; Mak, T. C. W. *J. Chem. Soc., Dalton Trans.* **1995**, 4001−4004.
(45) A rigid macrocyclic Schiff base contributes to the shortening of the 4.82 Å Mn···Mn distance (see ref 43).
(46) Baumeister, U.; Hartung, H.; Kaplonek, R. *Acta Crystallogr.* **1999**, *C55*, 715−717.
(47) Lis, T.; Matuszewski, J. *Acta Crystallogr.* **1979**, *B35*, 2212−2214.
(48) Zou, J.-Z.; Xu, Z.; Chen, W.; Lo, K. M.; You, X.-Z. *Polyhedron* **1999**, *18*, 1507−1512.
(49) Bonadies, J. A.; Kirk, M. L.; Soo Lah, M.; Kessissoglou, D. P.; Hatfield, W. E.; Pecoraro, V. L. *Inorg. Chem.* **1989**, *28*, 2037−2044.
(50) Zhang, K.-L.; Xu, Y.; Zheng, C.-G.; Zhang, Y.; Wang, Z.; You, X.-Z. *Inorg. Chim. Acta* **2001**, *318*, 61−66.
(51) Davies, J. *J. Chem. Soc., Dalton Trans.* **1973**, 2523−2527.

Table 4. Parameter Values for Calculation of Powder X-Band Spectra of $\mathbf{1}(ClO_4)_2$

T (K)	g_{iso}	D (cm^{-1})	E/D	ω_x (mT)	ω_y (mT)	ω_z (mT)	no. of points	Sophe grid
25	2.0	0.118	0.03	30	30	20	2048	80×80
293	2.0	0.102	0.03	28	28	20	2048	80×80

isotropic with a $g = 2$ value. The two experimental spectra can be satisfactorily reproduced with the same E/D ratio, the breath of the signal around $g = 2$ upon variation of the temperature being related to different D values. According to the temperatures at which the spectra were recorded, no temperature effects within the $S = 5/2$ manifold can be detected, and only the absolute value of the D parameter can be determined. Parameters for calculated spectra are listed in Table 4. The zero-field splitting effect is found quasi-axial ($E/D = 0.03$), which is not unexpected according to the X-ray structure. The $|D|$ value increases from 0.102 cm^{-1} at 295 K to 0.118 cm^{-1} at 25 K. This is puzzling according to the similarity of the X-ray structures determined at 110 K and at room temperature. However, a similar effect has been reported for the Mn(II)-doped $[Zn(DPA)_2](ClO_4)_2$ (DPA = bis(2-pyridylmethyl)amine) where the D parameter varies from -0.2190 to -0.2365 cm^{-1} between 298 and 77 K.[52] DFT calculations are planned to settle this point. For the calculated spectra, the manganese hyperfine interaction was neglected in eq 1 for computational purposes but also because no hyperfine structure was resolved on the experimental signals. The hyperfine interaction should split one line into six lines that present the same intensities and that can hardly be reproduced all together by a single line with a Gaussian or a Lorentzian line shape. However, the Mn hyperfine interaction will not strongly influence the positions of the transitions that only depend on the g, D, and E parameters, except on the low-field edge of the spectrum, where the Zeeman and hyperfine interactions are competitive. Indeed, as can be seen in Figure 2, the greater discrepancy between the calculated and experimental X-band EPR spectra is observed below 150 mT. Computational work is currently in progress to improve the EPR simulations.

The X-band spectra of $\mathbf{2}(ClO_4)_3 \cdot 2H_2O$ were recorded on a powder sample between 8 and 295 K. The 8 K spectrum, shown in Figure 2 (trace c), exhibits an intense line near $g = 2$ with less intense features on both the low-field (50, 150, and 255 mT) and high-field (535 and 630 mT) edges (see insets in Figure 2). When the temperature is increased, the profile remains almost unchanged and a general loss in intensity is observed (data not shown). At room temperature, the spectrum reduces to the line at $g = 2$ and a weaker one at 160 mT. The relative intensities of the spectra recorded below 295 K compared to the one at 295 K are lower than what is excepted if the observed signal follows a Curie-law dependence. These X-band traces differ strongly from those observed for the mononuclear complex $\mathbf{1}(ClO_4)_2$, indicating that the two Mn(II) ions in **2** are magnetically interacting. Recently, detailed analyses of the EPR signatures of dinuclear Mn(II) systems have been published.[53−56] The investigated species present stronger antiferromagnetic exchange interactions than in **2** (between -3 and -10 cm^{-1} vs -0.65 cm^{-1}). However, the common characteristic of the X- and Q-band EPR spectra observed when the temperature is increased is a gain in intensity in the $g = 2$ region, while features observed outside this region vanish (perpendicular detection mode). Such behavior is due to the decreasing contributions of the $S = 1-4$ excited spin states and the increasing participation of the $S = 5$ excited spin state. These manifolds are characterized by decreasing zero-field splitting effects as the S value increases, leading to an overlap of the EPR transitions in the $g = 2$ region. In addition, the higher the S value, the higher the intensity of the temperature-independent EPR S-spin signature. Consequently, the observed X-band EPR signal of **2** is characteristic of an antiferromagnetically coupled Mn(II) pair with a main contribution of the $S = 3-5$ spin states in the investigated temperature domain. The $\Delta M_S = \pm 1$ transitions are clustered in the $g = 2$ region, while the $\Delta M_S = \pm 2$ transitions gather around 160 mT. The detection of broad transitions makes intricate a detailed simulation of the EPR signature of $\mathbf{2}(ClO_4)_3 \cdot 2H_2O$ that would require at least consideration of the zero-field splitting effect of both metallic sites, the weak antiferromagnetic exchange interaction, the dipolar coupling, and the Zeeman interaction, all being of the same magnitude. The first attempts show that the local zero-field splitting tensors and the dipolar coupling tensor are probably not collinear. This increases the number of unknowns, and we postpone the detailed calculation of the EPR spectra.

EPR spectra were recorded on frozen acetonitrile solutions of $\mathbf{1}(ClO_4)_2$ and of $\mathbf{2}(ClO_4)_3 \cdot 2H_2O$. Surprisingly, the two EPR signals are very close (see trace a in Figures 4 and 7). The profile of the EPR spectrum of the acetonitrile solution of $\mathbf{1}(ClO_4)_2$ is pretty similar to the one recorded on the solid state, with the exception of the disappearance of the 65 mT line, the increase of the 160 mT transition, and the shift toward higher magnetic fields of the lines above 400 mT. The latter point can be attributed to a slight increase of the $|D|$ value. The changes observed on the low-field edge may originate from a D-strain effect due to a distribution of closely related complexes in solution. A distribution of the Mn hyperfine parameters may also contribute to the modifications of the signal of **1**. According to the similarity of the EPR signatures of **1** in the solid state and in solution, we propose that **1** remains heptacoordinated in acetonitrile. The generation of $[(tpen)Mn(NCCH_3)]^{2+}$ where the solvent

(52) Glerup, J.; Goodson, P. A.; Hodgson, D. J.; Michelsen, K.; Nielsen, K. M.; Weihe, H. *Inorg. Chem.* **1992**, *31*, 4611−4616.
(53) Blanchard, S.; Blondin, G.; Rivière, E.; Nierlich, M.; Girerd, J.-J. *Inorg. Chem.* **2003**, 4568−4578.
(54) Blanchard, S.; Blain, G.; Rivière, E.; Nierlich, M.; Blondin, G. *Chem.—Eur. J.* **2003**, 4260−4268.
(55) Pierce, B. S.; Elgren, T. E.; Hendrich, M. P. *J. Am. Chem. Soc.* **2003**, *125*, 8748−8759.
(56) Golombek, A. P.; Hendrich, M. P. *J. Magn. Reson.* **2003**, *165*, 33−48.

replaces the coordinated water molecule in the starting complex $[(tpen)Mn(OH_2)]^{2+}$ cannot be excluded on the basis of EPR analysis alone. It has to be noted that the 100 K X-band spectrum reported for a frozen acetonitrile solution of $[\{(tpen)Mn_3(\mu\text{-}O)_4(OH)\}_2(\mu\text{-}tpen)]^{6+}$ [37] is identical to that of **1** depicted here, with an additional contribution centered at $g = 2$ due to a slight amount of a mixed-valence Mn^{III}-Mn^{IV} complex. However, the generation upon dissolution of $\mathbf{1}(ClO_4)_2$ in acetonitrile of a Mn(IV)-based polynuclear complex is denied by the lack of absorption bands in the visible region (see part a of Figure S2).

The X-band EPR signature of **2** strongly differs in the solid state and in frozen acetonitrile. As shown on trace a of Figure 7, the previously described $g = 2$ signal is detected together with the signature of **1**. Consequently, we propose that the mono-acetato bridge of **2** partially breaks upon dissolution, leading to the generation of heptacoordinated Mn(II) complexes where tpen acts as a hexadentate chelating ligand, the seventh position being occupied by either a water or a solvent molecule or even the acetate anion. The three systems would be indistinguishable by EPR according to the similarity of the manganese coordination spheres. From the comparison between the intensities of the 180 and 645 mT lines detected on frozen solutions of complexes **1** and **2** when the EPR spectra are recorded using the same set of acquisition parameters, it appears that 75% of the Mn(II) ions initially introduced are incorporated into mononuclear EPR-active $[(tpen)Mn(X)]^{1+/2+}$ ($X = AcO^-$, H_2O, CH_3CN) systems.

Cyclovoltammetry. The cyclovoltammograms of complexes $\mathbf{1}(ClO_4)_2$ and $\mathbf{2}(ClO_4)_3 \cdot 2H_2O$ were recorded in acetonitrile (1 mM) with 0.1 M tetrabutylammonium perchlorate as a supporting electrolyte. The results are reported in Figure 3. One irreversible oxidation wave is detected on the cyclovoltammogram of **1** with $E^p = 1.5$ V vs SCE (solid line in part a of Figure 3). It may be attributed to the one-electron oxidation of $[(tpen)Mn(X)]^{2+}$ ($X = H_2O$ or CH_3CN). The addition of 2 equiv of 2,6-lutidine (also called 2,6-dimethylpyridine) per molecule of **1** leads to the increase in intensity of the first oxidation wave with a slight shift to lower potentials (dashed line in part a of Figure 3). This shift suggests that the added base reacts with the oxidized species following an EC mechanism.[57] Indeed, a new intense oxidation wave is detected at 1.75 V vs SCE upon the addition of 2,6-lutidine. The latter is attributed to the oxidation of a hydroxo-manganese(III) species, issued from the deprotonation of $[(tpen)Mn(OH_2)]^{3+}$ by 2,6-lutidine. In addition, the second oxidation wave contributes to the increase of the intensity of the first one. On the reverse scan, two small cathodic waves are observed at 0.6 and 0.25 V. One shall notice that these two waves are not observed when the potential is reversed at 1.65 V.

The cyclic voltammogram of complex **2** presents two irreversible oxidation waves at $E^p = 0.95$ V and $E^p = 1.5$ V vs SCE (see part b of Figure 3, solid line). The latter is

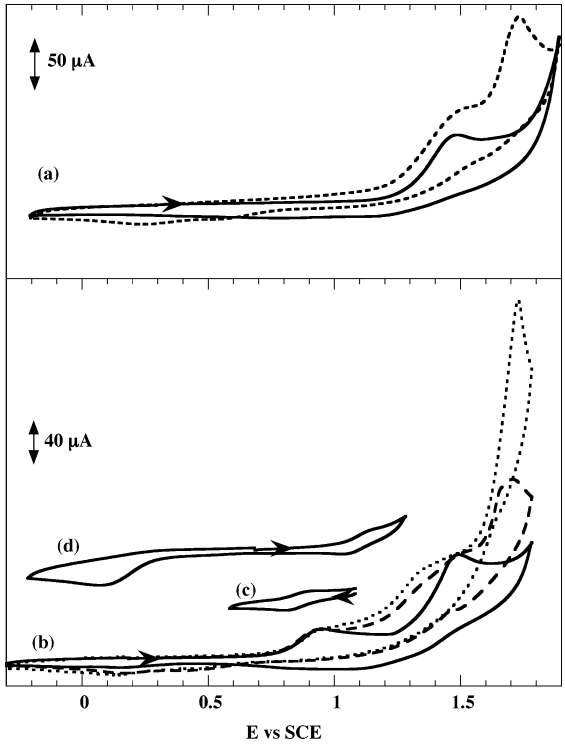

Figure 3. Cyclovoltammograms recorded for 2 mM acetonitrile solutions of $\mathbf{1}(ClO_4)_2$ (a) and $\mathbf{2}(ClO_4)_3 \cdot 2H_2O$ (b−d) with 0.1 M tetrabutylammonium perchlorate ($T = 20$ °C, $v = 100$ mV·s^{-1}): (a) **1** with (dashed line) or without (solid line) 2 equiv of 2,6-lutidine per manganese ion, (b) **2** with 2 (short dashed line), 1 (long dashed line) or 0 (solid line) equiv of 2,6-lutidine per manganese ion, (c) after bulk electrolysis of **2** at 1.1 V vs SCE in the presence of 1.3 equiv of 2,6-lutidine per Mn, (d) after bulk electrolysis of **2** at 1.1 V vs SCE in the presence of 2.65 equiv of 2,6-lutidine per Mn.

attributed to the presence of the mononuclear complex $[(tpen)Mn(X)]^{2+}$ ($X = H_2O$ or CH_3CN) formed, as suggested by EPR, by the breaking of the acetato bridge of **2** upon dissolution. The first oxidation wave can be attributed to the one-electron oxidation of either the mononuclear complex $[(tpen)Mn(OAc)]^+$ or the dinuclear species $[(tpen)Mn(\mu\text{-}OAc)Mn(tpen)]^{3+}$ (**2**). On the basis of the charge of these species, the mononuclear monocationic complex is favored. The addition of 2,6-lutidine up to 4 equiv per molecule of **2** modifies drastically the cyclic voltammogram. The first irreversible oxidation wave at $E^p = 0.95$ V vs SCE is unchanged, and a new irreversible and broad oxidation wave at $E^p = 1.35$ V vs SCE is detected as well as the intense and narrow wave at 1.75 V vs SCE previously mentioned (short and long dashed lines in part b of Figure 3). As in the case of **1**, the addition of 2,6-lutidine to the medium leads to a modification of the oxidation wave of $[(tpen)Mn(X)]^{2+}$ as observed by the increase in intensity at 1.35 V vs SCE. We cannot exclude that oxidation of free acetate ions may contribute to this increase ($E^p = 1.2$ V vs SCE). Indeed, the presence of base and condensation processes (see below) may induce the release of acetate ions at the Mn(III) level.

Bulk Electrolysis of 1. Electrolysis of a 2 mM acetonitrile solution of $\mathbf{1}(ClO_4)_2$ was performed at $E = 1.59$ V vs SCE. When no additional base is added to the medium, a passivation of the working electrode is observed quickly after the oxidative potential is turned on. On the other hand, the bulk electrolysis can be completed when 2 equiv of 2,6-

(57) We favor the action of 2,6-lutidine at the Mn(III) rather than the Mn(II) level.

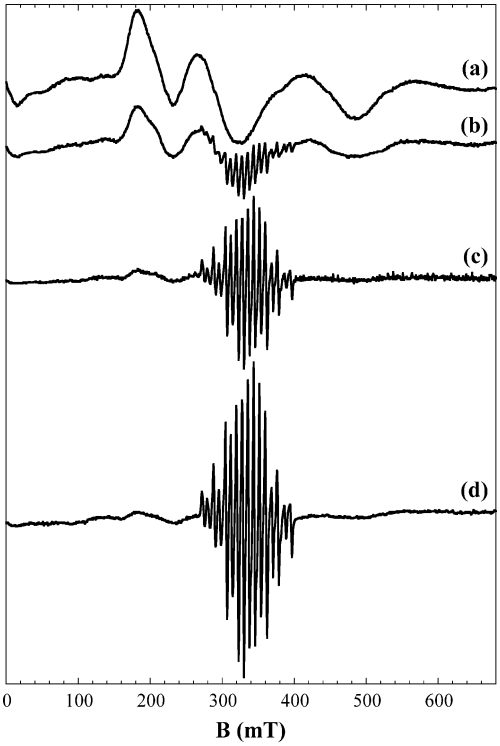

Figure 4. Series of X-band EPR spectra recorded on 100 μL aliquots taken during the course of the electrolysis of a 2 mM acetonitrile solution of **1**$(ClO_4)_2$ with 2.0 equiv of 2,6-lutidine per molecule of **1**. The numbers of exchanged electrons per manganese ion are (a) 0, (b) 1.03, (c) 2.06, and (d) 2.58. Recording conditions: 9.39 GHz microwave frequency, 2 mW microwave power, 0.5 mT modulation amplitude, 100 kHz modulation frequency, $T = 100$ K.

lutidine per manganese ion is added to the starting solution. Aliquots of 100 μL of the solution were regularly taken and the corresponding EPR spectra recorded (see Figure 4). The starting signature of the heptacoordinated complexes $[(tpen)Mn(X)]^{2+}$ ($X = OH_2$ or $NCCH_3$) decreases with the concomitant increase of a 16-line signal centered at $g = 2$. The spectral width measured as the first peak to last trough separation equals 125 mT, indicating the formation of a $[Mn^{III}(\mu\text{-}O)_2Mn^{IV}]^{3+}$ core complex that will be designated **3** in the following section. However, after 2.6 electrons per molecule of **1** are transferred, 10% of the starting signal remains. Aliquots were also regularly taken and the UV−vis spectra recorded. The starting spectrum presents one band at 260 nm ($\epsilon = 19150\ M^{-1}\ cm^{-1}$) with a shoulder at 270 nm ($\epsilon = 12340\ M^{-1}\ cm^{-1}$) that both originate from $\pi \rightarrow \pi^*$ transitions within the ligand. No band in the visible region is detected, as expected for a Mn(II) complex. Upon oxidation, four new bands at 300, 445, 555, and 660 nm are detected that increase during the course of the electrolysis. The molar extinction coefficients calculated per Mn ion when 2.7 electrons per molecule of **1** were exchanged are 4750, 525, 200, and 149 $M^{-1}\ cm^{-1}$, respectively (see Figure S2). These values are reminiscent of the ones usually observed for mixed-valence $[Mn^{III}(\mu\text{-}O)_2Mn^{IV}]^{3+}$ core complexes. For instance, the main features in the visible region for $[(Me_2\text{-bispicen})Mn(\mu\text{-}O)_2Mn(Me_2bispicen)]^{3+}$ (where Me_2bispicen is the *N*,*N*′-dimethyl-*N*,*N*′-bis(2-pyridylmethyl)-1,2-ethanediamine) are at 445, 555, and 661 nm with ϵ values per Mn ion of 446, 202, and 200 $M^{-1}\ cm^{-1}$, respectively.[58] The molar extinction coefficient value at 660 nm indicates that conversion of the starting mononuclear Mn(II) complex into **3** is not complete, in agreement with the EPR investigations. Furthermore, on the basis of the same absorption at 660 nm, the ϵ value at 445 nm is slightly larger than the expected one, suggesting that a small amount of the $[Mn^{IV}(\mu\text{-}O)_2Mn^{IV}]^{4+}$ core complex is jointly formed.[58] Indeed, the major change in the UV−vis spectrum when a $[Mn^{III}(\mu\text{-}O)_2Mn^{IV}]^{3+}$ core complex is oxidized to the corresponding $[Mn^{IV}(\mu\text{-}O)_2Mn^{IV}]^{4+}$ occurs below 500 nm.[59] This may contribute to the high value of the charge transferred measured during the electrolysis. Moreover, an electrolysis was run on a 10 mM solution of **1**, and a fine powder precipitated and was collected. We will show below that this powder indeed corresponds to the mixed-valence $[Mn^{III}(\mu\text{-}O)_2Mn^{IV}]^{3+}$ core complex **3** for which in addition a precise chemical formulation is given. The EPR spectrum recorded when the isolated powder was dissolved in acetonitrile corresponds to the 16-line signal with a 125 mT spectral width (data not shown). A close inspection of the infrared spectrum reveals the presence between 1500 and 1650 cm^{-1} of vibration modes of coordinated pyridine rings together with those of free pyridine groups (see Figure 5). From the comparison with the infrared signatures of the free tpen and of the ancillary bridging tpen in $[(tpen)Mn(\mu\text{-}O)_2(\mu\text{-}OAc)Mn](ClO_4)_2{\cdot}3H_2O$, the vibration mode at 1608 cm^{-1} is attributed to Mn-coordinated pyridine rings and the one at 1592 cm^{-1} to uncoordinated ones. This suggests the presence in **3** of more than one tpen ligand, since one can expect all the pyridine rings to be ligated if there is only one single ligand per dinuclear manganese core, as is observed in $[(tpen)Mn(\mu\text{-}O)_2(\mu\text{-}OAc)Mn]^{2+}$. Electrospray mass spectrometry measurements performed on a freshly prepared acetonitrile solution reveal one *m*/*z*-peak at 1188.3 with an isotopic pattern corresponding to a monocationic species. Such a high value can only be explained by the presence of two tpen ligands. A theoretical calculation of the isotopic profile of the monocation $\{[(tpen)Mn(\mu\text{-}O)_2Mn(tpen)](ClO_4)_2\}^+$ perfectly

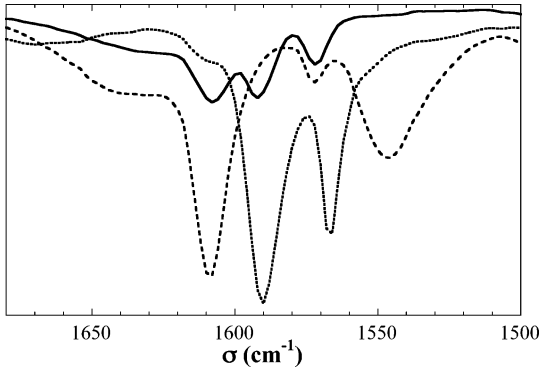

Figure 5. Infrared spectra in the 1680−1500 cm^{-1} region of the tpen ligand (dotted line), $[(tpen)Mn(\mu\text{-}O)_2(\mu\text{-}OAc)Mn](ClO_4)_2$ (dashed line), and $[(tpen)Mn(\mu\text{-}O)_2Mn(tpen)](ClO_4)_3$ (**3**$(ClO_4)_3$) (solid line).

(58) Goodson, P. A.; Glerup, J.; Hodgson, D. J.; Michelsen, K.; Weihe, H. *Inorg. Chem.* **1991**, *30*, 4909−4914.
(59) Horner, O.; Charlot, M.-F.; Boussac, A.; Anxolabéhère-Mallart, E.; Tchertanov, L.; Guilhem, J.; Girerd, J.-J. *Eur. J. Inorg. Chem.* **1998**, 721−727.

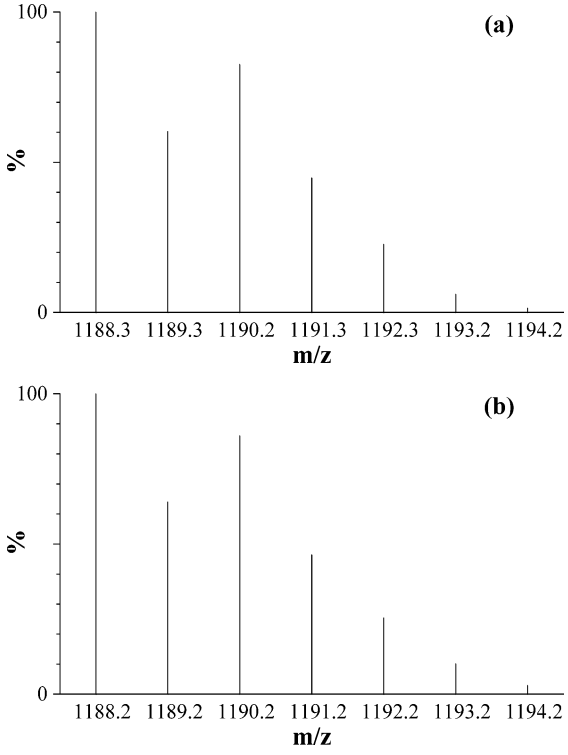

Figure 6. Experimental (a) and theoretical (b) isotopic profiles detected at $m/z = 1188.3$ by electrospray mass spectrometry on an acetonitrile solution freshly prepared from the powder isolated at the end of the bulk electrolysis of **1**$(ClO_4)_2$ in the presence of 2 equiv of 2,6-lutidine per molecule of **1**.

Chart 1. Schematic View of **3**

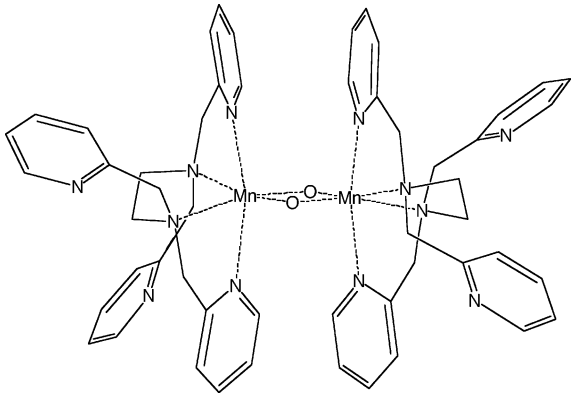

matches the experimental detected one (see Figure 6). In conclusion, the bulk electrolysis of **1**$(ClO_4)_2$ in the presence of 2 equiv of 2,6-lutidine per manganese ion leads to the formation of the mixed-valence $Mn^{III}Mn^{IV}$ complex $[(tpen)Mn(\mu\text{-}O)_2Mn(tpen)]^{3+}$ (**3**). In **3**, the tpen ligand would act as a tetradentate ligand with two uncoordinated pyridylmethyl arms per ligand. A schematic view is given in Chart 1.

Bulk Electrolysis of 2. Electrolyses of a 1.8 mM acetonitrile solution of **2**$(ClO_4)_3 \cdot 2H_2O$ were performed at $E = 1.1$ V vs SCE with different amounts of additional 2,6-lutidine, ranging between 0 and 2.65 per Mn ion. When 2.65 equiv is added to the starting solution, the EPR spectra recorded on 100 μL aliquots that were periodically taken indicate the continual decrease of the starting signal with the concomitant increase of the same 16-line signal described above (data not shown). We thus suspect the formation of the same mixed-valence $[Mn^{III}(\mu\text{-}O)_2Mn^{IV}]^{3+}$ core complex **3**. The cyclovoltammogram was recorded at the end of the electrolysis and is reproduced in Figure 3 (see trace d). The starting stable potential is 0.68 V vs SCE. When scanning is done toward higher potentials, one reversible oxidative wave is detected with the associated reductive process on the reverse scan at $E^{1/2} = 1.08$ V vs SCE ($\Delta E^p = 0.08$ V). One irreversible reduction wave is also detected at $E^p = 0.07$ V vs SCE. The reversible process can be associated with the exchange of one electron between the III−IV and IV−IV oxidation states of the generated dimanganese−di-μ-oxo complex. However, it is surprising that the redox process between the $[Mn^{III}(\mu\text{-}O)_2Mn^{IV}]^{3+}$ and the one-electron-reduced form $[Mn^{III}(\mu\text{-}O)_2Mn^{III}]^{2+}$ is not reversible. This will be addressed at a later point in the Discussion. When the electrolysis was performed on a more concentrated solution of the dinuclear complex **2** (3.2 mM) in the presence of more than 4 equiv of 2,6-lutidine, a fine powder formed and was collected. The complete set of characterizations (infrared, UV−vis, EPR, and electrospray) were performed on the isolated powder, demonstrating that the mixed-valence complex $[(tpen)Mn(\mu\text{-}O)_2Mn(tpen)]^{3+}$ shown in Chart 1 is formed upon oxidation and isolated as the perchlorate salt **3**$(ClO_4)_3$.

Bulk electrolyses of **2**$(ClO_4)_3 \cdot 2H_2O$ were also performed with decreasing amounts of 2,6-lutidine. A typical series of collected X-band EPR spectra are reproduced in Figure 7. A scrupulous examination of the recorded series indicates that the increase of the 16-line signature of the mixed-valence complex **3** occurs first with the concomitant decrease of the $g = 2$ line (see traces b and c of Figure 7) and second with the decrease of the EPR signature of mononuclear heptacoordinated Mn(II) species. The main difference with the previously described experiment for which 2.65 equiv of 2,6-lutidine has been introduced is the decrease of the 16-line signal before the completion of the electrolysis. When the electrolysis is completed, the final EPR spectrum presents almost no signal in the $g = 2$ region and a significant proportion of the starting signal is detected. The latter originates from heptacoordinated Mn(II) complexes that account for 25−40% of the initially introduced metallic ions, with the exception of the experiment performed without additional base where the value reaches 65%. We may conclude from these data that the mixed-valence dinuclear di-μ-oxo complex **3** is indeed formed upon oxidation but further evolves into an EPR-silent species, **4**. All the electrolyses performed were pursued until 2.1−2.2 electrons per manganese ion were exchanged, with the exception of the experiments performed without additional base for which the current faded after the exchange of 0.9 electron per Mn. This low value is at the origin of the more intense EPR signature of mononuclear Mn(II) species detected at the end of the electrolysis. The maximum in intensity of the 16-line signal detected during the course of the electrolysis decreases as the amount of extra base in the starting solution decreases. The amount of **3** may be reproduced by the number of exchanged electrons per Mn. The variation of the exchange electrons per Mn ion at the maximum in intensity of the 16-

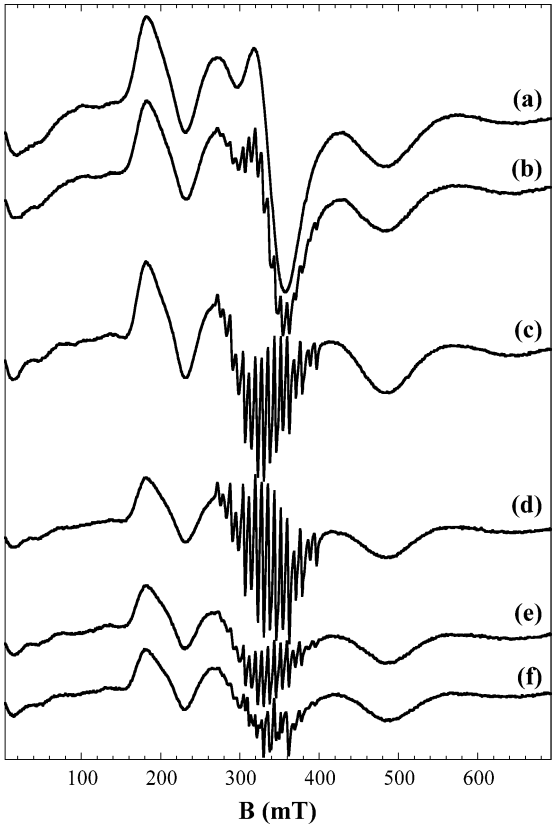

Figure 7. Series of X-band EPR spectra recorded on 100 μL aliquots taken during the course of the electrolysis of a 1.8 mM acetonitrile solution of **2**$(ClO_4)_3 \cdot 2H_2O$ with 1.3 equiv of 2,6-lutidine per manganese ion. The numbers of transferred electrons per manganese ion are (a) 0, (b) 0.35, (c) 0.73, (d) 1.17, (e) 1.90, and (f) 2.19. Recording conditions: 9.388 GHz microwave frequency, 2 mW microwave power, 0.5 mT modulation amplitude, 100 kHz modulation frequency, $T = 100$ K.

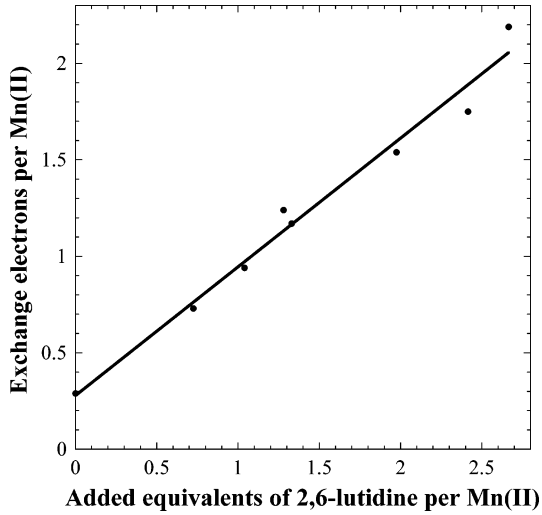

Figure 8. Number of exchanged electrons per introduced Mn(II) ion corresponding to the maximum of the detected 16-line X-band signal as a function of the number of equivalents of 2,6-lutidine added per Mn(II) ion when an acetonitrile solution of **2**$(ClO_4)_3 \cdot 2H_2O$ is electrolyzed at 1.1 V vs SCE. The solid line is a linear fit of the experimental data points (see the text).

line spectrum is reproduced in Figure 8 as a function of the additional base. The points indeed form a straight line, and a linear fit leads to a slope of 0.67 electron per added molecule of 2,6-lutidine. By looking at the overall equation summarizing the oxidation of the starting mono- or dinuclear Mn(II) complex **1** or **2** into the mixed-valence species **3** that requires 1.5 electrons per manganese ion, the generation of 2 protons per manganese ion is clearly evidenced (see eq 2). Thus, the theoretical ratio of the abstracted electrons per external base added to neutralize the generated protons is 0.75. Consequently, the 0.67 determined value is in perfect agreement with the proposed redox process.

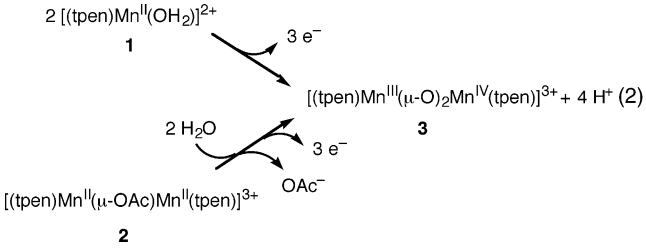

On the other hand, the generated EPR-silent species **4** forms all the earlier during the electrolysis than when the external base is introduced in small quantity. This means that species **4** is indeed the most favored oxidized form of the system, addition of 2,6-lutidine preventing its formation. The UV−vis spectra reveal absorption bands in the visible region with an important increase around 450 nm and around 600 nm with the concomitant decrease between 700 and 750 nm, suggesting the formation of a Mn^{IV}-oxo system (see Figure S2). From EPR and UV−vis spectra, the formation of a dinuclear Mn(IV) species, **4**, may be proposed. The cyclovoltammogram recorded at the end of the electrolysis performed with 1.3 equiv of base per Mn ion is shown in Figure 3 (see trace c). Upon scanning toward negative potentials, it presents a reversible reduction wave with the associated oxidation process at $E^{1/2} = 0.86$ V vs SCE ($\Delta E^p = 0.09$ V). This $E^{1/2}$ value is lower than the one at 1.08 V vs SCE associated with the [(tpen)$Mn^{III}(\mu$-O)$_2Mn^{IV}$(tpen)]$^{3+}$/[(tpen)$Mn^{IV}(\mu$-O)$_2Mn^{IV}$(tpen)]$^{4+}$ redox couple but is close to the one previously reported for the [(tpen)$Mn^{III}(\mu$-O)$_2(\mu$-OAc)Mn^{IV}]$^{2+}$/[(tpen)$Mn^{IV}(\mu$-O)$_2(\mu$-OAc)Mn^{IV}]$^{3+}$ process ($E^{1/2} = 0.89$ V vs SCE).[37,60] According to the intensity of this redox wave, a concentration of 1 mM may be estimated for the dinuclear species [(tpen)$Mn^{IV}(\mu$-O)$_2(\mu$-OAc)Mn^{IV}]$^{3+}$, which corresponds to a 55% yield. This is indeed in agreement with the EPR studies: the ultimate recorded signal (trace f in Figure 7) originates from mononuclear Mn(II) complexes that account for 40% of the initially introduced Mn(II) ions. An irreversible oxidation wave is also detected at $E^p = 1.5$ V vs SCE when scanning is done toward higher potentials (not shown) which may correspond to the oxidation of the residual heptacoordinated Mn(II) complexes [(tpen)-$Mn^{II}(X)]^{2+}$ (X = H_2O, CH_3CN). Consequently, we propose that the EPR-silent species **4** formed is the dimanganese-(IV) complex [(tpen)Mn(μ-O)$_2$(μ-OAc)Mn]$^{3+}$. The mechanism of formation of **3** and **4** will be discussed below.

Discussion

The bulk electrolysis of an acetonitrile solution of **1**$(ClO_4)_2$ cannot be performed in the absence of 2,6-lutidine. When 2

(60) The literature value is reported vs SSCE. Conversion to that vs SCE is obtained by subtracting 5 mV.

equiv of base per manganese ion is added to the starting solution, the mixed-valence $[(tpen)Mn^{III}(\mu\text{-}O)_2Mn^{IV}(tpen)]^{3+}$ complex (**3**) is formed with one tpen ligand remaining coordinated per manganese center. The same complex is also generated when starting from **2**, even in the absence of additional base. Indeed, the acetate anion is a strong base in acetonitrile ($pK_a = 22$).[61] As for **1**, **3** is the resulting product of the bulk electrolysis on the condition that more than 2 equiv of 2,6-lutidine per manganese ion is introduced. When a smaller amount of base is added to a solution of **2**, an EPR-silent species, **4**, is ultimately formed. EPR and UV−vis spectroscopy together with cyclovoltammetry lead to the same conclusion that **4** is the di-μ-oxo-μ-acetato-dimanganese(IV) complex $[(tpen)Mn(\mu\text{-}O)_2(\mu\text{-}OAc)Mn]^{3+}$. The key feature is the lower tpen/Mn ratio in **4** compared to that in **3** or in the starting species **2** or **1**: 1/2 vs 1/1. In other words, the formation of the highest oxidized species **4** leads to the release of the tpen ligand, which may act as a base toward the protons released upon the formation of the oxo bridges originating from residual water molecules. The resulting complex is stabilized by the coordination of the acetate anion initially introduced with **2**. Consequently, the driving force of the electrolysis is the neutralization of these protons. When no additional base is added to the medium, the oxidation leads to the formation of **4**. The reaction generates four protons when four electrons are abstracted (see eq 3).

$$\underset{\mathbf{2}}{[(tpen)Mn^{II}(\mu\text{-}OAc)Mn^{II}(tpen)]^{3+}} \xrightarrow[\text{tpen}\quad 4\ e^-]{2\ H_2O} \underset{\mathbf{4}}{[(tpen)Mn^{IV}(\mu\text{-}O)_2(\mu\text{-}OAc)Mn^{IV}]^{3+}} + 4\ H^+ \qquad (7)$$

The four protons are partially neutralized by the tpen ligand being either free or coordinated to a manganese ion. In the last case, tpen acts as a tetra- or pentadentate ligand with at least one protonated dangling pyridine arm. The protonation of tpen in the $[(tpen)Mn(X)]^{1+/2+}$ complexes prevents the Mn^{II} to Mn^{III} oxidation process and the further chemical reactions from occurring, in agreement with the final recorded EPR signals. When an external base is added to the medium, the release of the tpen ligand is no longer required and a dinuclear complex presenting a 1/1 tpen/Mn ratio can be generated. The choice of the 2,6-lutidine was guided by the high value of its oxidation potential and its low capability to coordinate to a metal ion. We have recently shown its utility toward the electrochemical formation of new Mn−oxo complexes.[62] In other words, when 2,6-lutidine is added such as to neutralize all the protons released by the formation of the di-μ-oxo bridge, complex **3** is the final product. Two mechanisms for the formation of **3** can be considered, none of them being favored on the basis of the collected data. The simplest one is a direct one-electron oxidation of the dimanganese(III)−di-μ-oxo complex $[(tpen)Mn^{III}(\mu\text{-}O)_2Mn^{III}(tpen)]^{2+}$ as reported in the literature for a similar compound.[30] The second process relies on the well-known dismutation reaction between one $Mn^{III}(\mu\text{-}O)Mn^{III}$ motif and the protonated form $Mn^{III}(\mu\text{-}OH)Mn^{III}$.[63] Whatever the mechanism, the dinuclear Mn(III) species result from the condensation of the mononuclear Mn(III) species formed upon oxidation at 1.1 or 1.5 V vs SCE.

Acetate anions are responsible for the lowering of the applied potential to perform bulk electrolyses. The disappearance of the EPR line at $g = 2$ at the beginning of the bulk electrolyses of solutions of **2** can be interpreted by an increased fragility of the dinuclear complex $[(tpen)Mn^{II}(\mu\text{-}OAc)Mn^{II}(tpen)]^{3+}$ under oxidative conditions possibly due to a direct oxidation.

As previously mentioned, the reduction wave detected on the cyclovoltammogram is not reversible (see trace d in Figure 3). This may be attributed to the presence in solution of the protonated 2,6-lutidine that is acidic enough to protonate the di-μ-oxo bridge of the $[(tpen)Mn^{III}(\mu\text{-}O)_2Mn^{III}(tpen)]^{2+}$ complex. The pK_a value of the protonated 2,6-lutidine is near 14[64,65] in acetonitrile, and a value of 14.6 has been previously evaluated for the $[(phen)_2Mn^{III}(\mu\text{-}O)(\mu\text{-}OH)Mn^{III}(phen)_2]^{3+}$ complex.[66] We may thus expect a value close to 14 for $[(tpen)Mn^{III}(\mu\text{-}O)(\mu\text{-}OH)Mn^{III}(tpen)]^{3+}$. The generation at the electrode of the $[Mn^{III}(\mu\text{-}O)(\mu\text{-}OH)Mn^{III}]^{3+}$ core complex would be at the origin of the irreversible reduction wave of **3**.

The thorough investigation of the behavior of the dinuclear complex $[(tpen)Mn^{II}(\mu\text{-}OAc)Mn^{II}(tpen)]^{3+}$ (**2**) under oxidative potential reveals the versatility of the coordination of the tpen ligand together with its role as a base. Indeed we shall note that Armstrong et al. quoted the role of the excess ligand tpen as a base in the formation of the $[(tpen)Mn_2(\mu\text{-}O)_2(\mu\text{-}OAc)]^{2+}$ complex.[36] In the presence of acetate ions, the chemical nature of the dimanganese core, $(\mu\text{-}O)(\mu\text{-}OAc)_2$ vs $(\mu\text{-}O)_2(\mu\text{-}OAc)$, and thus the oxidation state of the manganese ions, is finely controlled by the acidobasicity of the reaction medium.[29]

Concluding Remarks

In this paper we have reinvestigated the coordination chemistry of the tpen ligand with Mn ions. Two heptacoordinated Mn(II) complexes have been crystallographically characterized, namely, $[(tpen)Mn(OH_2)]^{2+}$ (**1**) and $[(tpen)Mn(\mu\text{-}OAc)Mn(tpen)]^{3+}$ (**2**). We have shown that bulk electrolysis of **2** in the presence of 2,6-lutidine leads to the formation of two high-valent dimanganese complexes that

(61) Izutsu, K. *Acid−Base Dissociation Constants in Dipolar Aprotic Solvents*; Blackwell Scientific Publications: Brookline Village, MA, 1990; Vol. 35.
(62) Hureau, C.; Sabater, L.; Anxolabéhère-Mallart, E.; Nierlich, M.; Charlot, M.-F.; Gonnet, F.; Rivière, E.; Blondin, G. *Chem.—Eur. J.* **2004**, *10*, 1998−2010.
(63) Wieghardt, K.; Bossek, U.; Nuber, B.; Weiss, J.; Bonvoisin, J.; Corbella, M.; Vitols, S. E.; Girerd, J.-J. *J. Am. Chem. Soc.* **1988**, *110*, 7398−7411.
(64) Augustin-Nowacka, D.; Chmurzyñski, L. *Anal. Chim. Acta* **1999**, *381*, 215−220.
(65) Kaljurand, I.; Rodima, T.; Leito, I.; Koppel, I. A.; Schwesinger, R. *J. Org. Chem.* **2000**, *65*, 6202−6208.
(66) Larsen, A. S.; Wang, K.; Lockwood, M. A.; Rice, G. L.; Won, T.-J.; Lovell, S.; Sadilek, M.; Turecek, F.; Mayer, J. M. *J. Am. Chem. Soc.* **2002**, *124*, 10112−10123.

differ in their oxidation states, metal/ligand ratio, and core structures, namely, $[(tpen)Mn^{III}(\mu\text{-}O)_2Mn^{IV}(tpen)]^{3+}$ (**3**) and $[(tpen)Mn^{IV}(\mu\text{-}O)_2(\mu\text{-}OAc)Mn^{IV}]^{3+}$ (**4**). The ultimate formation of **3** vs **4** is accurately controlled by the amount of added base. In addition, this is the first time that the di-μ-oxodimanganese compound **3** has been reported. This mixed-valence complex can be electrogenerated from acetonitrile solutions of either complex **1** or complex **2** when 2 equiv of 2,6-lutidine per manganese ion is initially introduced.

We plan to investigate the evolution of the mononuclear Mn(II) complex **1** under oxidative potential when less than 2 equiv of 2,6-lutidine per molecule of **1** is introduced. According to the redox behavior of complex **2**, we may expect the partial release in solution of the tpen ligand concomitantly with the formation of the di-μ-oxo-dimanganese core unit. This should lead to a $[(tpen)Mn_2(\mu\text{-}O)_2]^{n+}$ complex with one labile position on each metallic site. Such a complex is of crucial interest with respect to the fixation of additional water molecules and/or the conversion toward higher nuclearity manganese complexes.

Acknowledgment. We are grateful to Félix Perez for mass spectrometry measurements. We thank the Conseil Régional de l'Ile de France for its contribution to the acquisition of the Bruker ELEXSYS X- and Q-band EPR spectrometer. The COST D21 European action and the LRC-CEA project are acknowledged for their financial support. Constructive comments of one reviewer significantly improved this paper. We deeply thank this person for the time spent to review this work.

Supporting Information Available: CIF files for the X-ray structure of $[(tpen)Mn(OH_2)](ClO_4)_2$ (**1**$(ClO_4)_2$) at 110 and 293 K and for $[(tpen)Mn(\mu\text{-}OAc)Mn(tpen)](ClO_4)_3 \cdot 2H_2O$ (**2**$(ClO_4)_3 \cdot 2H_2O$). Variation of the molar magnetic susceptibility χ_M with temperature plotted as a $\chi_M T$ vs T curve (Figure S1) and UV−vis spectra recorded upon electrochemical oxidation of **1** and **2** (Figure S2) (PDF). This material is available free of charge via the Internet at http://pubs.acs.org.

IC035332U